

Fluid-structure interaction for large scale complex geometry and non-linear properties of structure

R. ROSZAK, P. POSADZY, W. STANKIEWICZ,
M. MORZYŃSKI

*Poznan University of Technology
Institute of Combustion Engines and Transportation
Piotrowo 3, 60-965 Poznań, Poland
e-mail: roszak@stanton.ice.put.poznan.pl
morzynski@stanton.ice.put.poznan.pl
stankiewicz@stanton.ice.put.poznan.pl
posadzy@stanton.ice.put.poznan.pl*

IN THIS PAPER fluid-structure interaction, taking into account the nonlinearity of structural models, is concerned. This phenomenon has important influence in many aeronautical applications. The method and developed system is demonstrated on NACA-0012 wing mounting, made of non-linear springs and include structures with non-linear materials, modelled by Neo–Hooke and Mooney–Rivlin models, like flexible delta wing. For the first flow the comparison with experiment made in Institute of Aviation Warsaw is presented. For both mentioned above models, the linear and non-linear analysis are presented and the critical flutter speeds are determined. Finally, aeroelastic simulation of full I23 aircraft configuration presents the capability of used numerical codes to analyze large-scale complex geometries. All computations were carried out in parallel environment for CFD mesh of order of millions tetrahedral elements.

Copyright © 2009 by IPPT PAN

1. Introduction

EXPANSION OF COMPUTER TECHNOLOGIES allows using numerical simulation in the early stages of aircraft design more and more often. The role of both the wind tunnels and initial test flights used to verify the validity of solutions seems to be diminishing. Big systems for three-dimensional simulations of Fluid-Structure Interactions (FSI) constitute highly specialized and costly software. Most of the codes are based on many simplifications. One of them is the assumption of linearity of the structural model being in contradiction with real-life situations. What is meant by the non-linearity of structure is: a) geometrical non-linearity, in which case large deformations of the system cause the lack of the proportionality between load and displacement; the influence of displacement on static quantities; b) material non-linearity stemming from a constitutive equation. The paper presents the results of simulations for

complex, multi-scale objects and non-linear structure models. What is crucial for carrying out the assumed analyses is to extend a numerical tool [1] comprising a flow and a structural program and a space grid deformation model for a system allowing to take into consideration the non-linearity of structure.

The scope of our work has included:

- Joining independent programs: flow, structural, interpolation and three-dimensional CFD grid deformation tools into one integrated system.
- Adapting a structural code to a non-linear analysis and modifying FSI control script.
- Carrying out tests.
- Analyzing FSI on certain examples.
- Visualizing the results.

The point of reference for testing the suggested approaches are the existing solutions of the aeroelastic linear problems.

The paper is organized as follows. In Sec. 2 the brief description of Computational Aeroelasticity problems are presented. The Sec. 3 concerns possible nonlinearity types and their properties. The methodology of Fluid-Structure Interaction is given in Sec. 4, and demonstrated in Sec. 5. The examples include NACA-0012 profile (compared with Institute of Aviation Warsaw – IoA – experiment) and flexible delta wing. Finally, the developed and validated algorithm is demonstrated on full I23 aircraft configuration.

2. Computational Aeroelasticity

Computational Aeroelasticity [2] is a branch of mechanics which examines the way a stream of fluid affects a deformable body that it flows around. The term combines the methods used in Computational Fluid Dynamics (CFD) and Computational Structural Mechanics (CSM) [3]. The non-linearity found in structural models is usually not taken into consideration in numerical analyses of interacting fluid and structures found in the literature [2–5]. This limits the possibility of simulating such cases as maneuvers of planes, in which considerable deformation of structure occurs, and cases with the non-linearity of constitutive equation. The non-linearity is also of particular importance for biological flows as, for example, blood flow in the blood vessels [5].

Because of the wide scope of FSI, the paper is focused on fluid and structure interaction in external flows. Computational methods for different aspects of aeroelastic responses are still the subject of scientific examination. To illustrate the point, many aspects in [2] are FSI related to search interdependence between aerodynamics in a flow and the dynamics of structure. This approach is connected with many complications stemming from two independent numerical codes interacting with each other.

Another problem to be solved is the way of exchanging information between programs for fluids and structure (Fig. 1), with a different level of discretization and use of different methods (finite elements, finite volumes). One significant problem in analyses of FSI is the description of particular states in relation to two different coordinate systems used. What is used quite often [2] is use of Euler's description – a stationary coordinate system (CSM) or Lagrange's description – a movable coordinate system (CFD). Thus it is necessary to devise appropriate techniques of data exchange between these two systems.

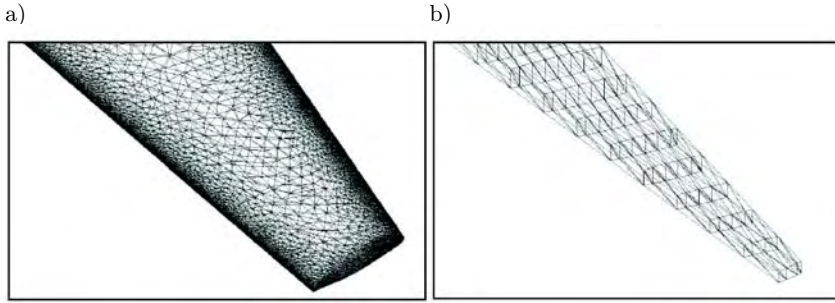


FIG. 1. An example of differences in discretization for the NACA 0012 airfoil: a) a CFD grid – tetrahedral elements, b) a structural grid – beam and surface elements.

What also poses a problem is adopting the time step in calculations which can be different for a flow code and for a structural code. It is particularly important when conducting a dynamic analysis of a FSI.

3. A non-linear structural problems

A numerical algorithm to carry out aeroelastic analyses consists of a flow program and a structural program. The paper presents the algorithm of aeroelastic calculations using non-linear structural models. To outline the question of a non-linear structural problem, let us consider the governing equations for the structure motion (3.1):

$$(3.1) \quad M\ddot{x} + C\dot{x} + Kx = F.$$

In linear problems the relationships between load and displacement are proportional. In the case of structural non-linearity (covering the scope of work), the last matrix of the left side of the Eq. (3.1) K is formulated through a function. K represents the stiffness matrix of the structure and for non-linear cases it is defined by a function of characteristic properties of a given material. The Eq. (3.2) for non-linear structural problems used in the case of work is as follows:

$$(3.2) \quad M\ddot{x} + C\dot{x} + K(x)x = F.$$

Matrix C represents the damping which can also be non-linear. Damping defined in this way together with the FSI algorithm can be applied in the flow control.

3.1. Non-linear material models used in simulations

In structural calculations for constitutive (material) non-linearity, a hyper-elastic material is used. On the basis of functions and introduced constants C_{10} and C_{01} , invariants I_1, I_2, I_3 are specified for a given non-linear material, in which the coordinates of the Cauchy–Green stress tensor, regardless of how the coordinate system has been specified [6]. Nowadays the commonly used non-linear material models in structural analyses are Arruda–Boyce’s, Mooney–Rivlin’s, Neo–Hookean, Odgen’s, Polynomial and Yeoh’s.

This paper outlines the approach towards non-linear material models formulated by Mooney–Rivlin and Hooke to analyse the FSI. Mooney–Rivlin’s material model is described through the function of energy of non-dilatational strain as follows [6]:

$$(3.3) \quad W = C_{10}(\bar{I}_1 - 3) + C_{01}(\bar{I}_2 - 3),$$

where W – the energy of the non-dilatational strain, \bar{I}_1, \bar{I}_2 – the combination of invariants I_1, I_2, I_3 of the Cauchy–Green strain tensor, C_{10}, C_{01} – material constants characteristic of a particular material [6].

The Mooney–Rivlin material model used in the paper is based on two invariants. In practice, it means the possibility of modelling most types of non-linear materials. The Neo–Hookean material model can be treated as a simplified version of the Mooney–Rivlin model. The function of energy of the non-dilatational strain is as follows:

$$(3.4) \quad W = C_{10}(\bar{I}_1 - 3),$$

where W – the energy of the non-dilatational strain, \bar{I}_1, \bar{I}_2 – the combination of invariants I_1, I_3 of the non-dilatational strain, C_{10}, C_{01} – the material characteristic constants of a given material [6].

4. The fluid structure interaction algorithm

There are many methods to perform fluid-structure interaction computations. In the first approach, equations describing all the coupled physical phenomena are coupled in one code. As each of components of the coupled problem has different mathematical and numerical properties (linear/non-linear equations, symmetric/unsymmetric matrices, etc.), [7], this approach is computationally challenging. The alternative approach, used in this work, is based on

the code coupling, where fluid flow computations and structural analyses are performed by separate packages. Depending on the the particular problem, different numerical strategies might be employed. The overview of them might be found in pioneer studies by FARHAT, PIPERNO and others [7–9].

To carry out aeroelastic calculations, a control system has been created which has interrelated particular numerical tools into one integrated system. The designed control scripts allow efficient calculations. The program starts with static analysis, then the perturbation of the solution is introduced and dynamic analysis continues.

The following tools have been used in the presented system.

4.1. TAU-Code

For CFD computations, a parallel and efficient RANS flow code (Reynolds Averaged Navier–Stokes) by Deutsches Zentrum fuer Luft- und Raumfahrt (DLR) [10], has been used. The system consists of two modules: the first one is used to prepare a task for calculations (pre-processing): the checking of the grid, the division into subdomains (in the case of parallel calculations), the introduction of boundary conditions, etc.; the second one solves a system of equations (Euler’s or RANS if turbulence and viscosity are taken into account).

4.2. The deformation module

It is a module for modifying a CFD grid on the basis of the deformation of the structure; the aim of this modification is to change the CFD grid in such a way that the points (nodes) of the coupling surface lie on the surface of the object being flown round, while preserving the quality of the mesh.

Multiple methods used for mesh deformation incorporate the spring analogy concept. All of them are based on the assumption, that the tetrahedral (cubic, etc.) elements of the CFD mesh are replaced with spring elements. The difference between them is the number of interpolation triangles that are activated in each case. Among these methods, torsional spring analogy [11, 12], semi-torsional spring analogy [13, 14], ortho-semi-torsional (OST) spring analogy [15] and ball-vertex spring analogy [16] can be mentioned. For the purpose of aeroelastic computations the efficient mesh deformation system has been developed. It is based on in-house MF3 structural code and beam elements. It combines benefits of spring and torsional orthotropic spring analogy.

4.3. The MF3 structural code

For elastic calculations MF3 [17] – the in-house finite-element code has been used. It allows static and dynamic calculations and a modal analysis using

1-dimensional (beams, rods), 2-dimensional (shells, membranes, etc.) and 3-dimensional (tetrahedral, hexahedral) elements.

4.4. The F2S and S2F modules

The fluid-structure interaction algorithm, used in aeroelasticity analyses, requires the transfer of some quantities between the used codes. In the interaction mentioned before, pressures computed in CFD software act as the loads in structural code. The deformations of structural mesh, resulting from CSM analyses, influence the computational domain and the boundary conditions in the CFD part of the coupled system.

The interpolation algorithms are divided into the ones based on the geometry and the other ones based on the finite element mesh. The example of the first group is spline interpolation [18, 19]. The codes based on the definitions of mesh points [20, 21] usually define the surfaces, where the interaction between coupled codes occurs. Due to the fact that coupled software is multidisciplinary, and the domain used in structural analysis may be not rigid, the interpolation tools have to determine how the coupling surfaces of both domains fit together [21].

There are several different search algorithms aimed at finding the adequate pairs of points and elements on the coupling surfaces. One of the most straightforward of them is linear search, shown in [22]. As it has been described in [21], the computational cost of the comparison of all pairs of points rapidly increases with the growth of mesh size. Other methods, e.g. oct-tree [23, 24] and bucket [25–27] search algorithms, are based on restricting the search region and are much more efficient. The detection strategies differ for matching and non-matching meshes. In the first case, the structure of the both contact surfaces is the same, and only the pairs of points have to be found. For different levels of discretization or in case when the geometry in one of the coupled tools is simplified, the algorithm for non-matching grids has to be used. In this case, the pairs of points and elements have to be found. Again, bucket and oct-tree algorithms are more efficient than the linear search.

When the neighborhood of the points and elements is computed, the interpolation can be performed. Depending on the type of the quantity to be interpolated, different methods can be mentioned:

- Non-conservative interpolation might be used for the functions of spatial coordinates in time, like the pressures, velocities or the mesh points coordinates.

In the case of non-conservative interpolation (Fig. 2), for each point of target mesh the corresponding element on the source mesh is found. Next, the values from source points are interpolated to the target point (lying inside the source element).

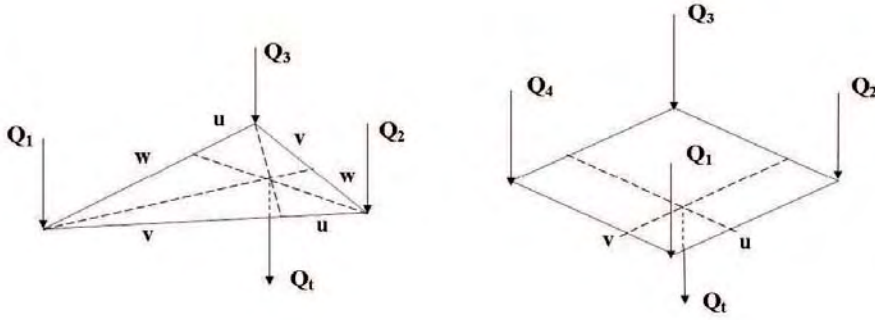


FIG. 2. Non-conservative interpolation. Data are interpolated from source points Q_i to a target point Q_t .

- Conservative interpolation is adequate in the cases, when some additional laws must be preserved during interpolation. The example of such situation is the interpolation of the forces, when their sum has to be preserved. In that case (Fig. 3), the source value is located in a single point and transferred to the points of element lying on target coupling surface, using weights w_i that satisfy $\sum_i w_i = 1$. Each node on target element gets a portion $w_i \cdot Q_t$ of the given coupling quantity.

For interpolation in the system presented here, three sets of modules were tested.

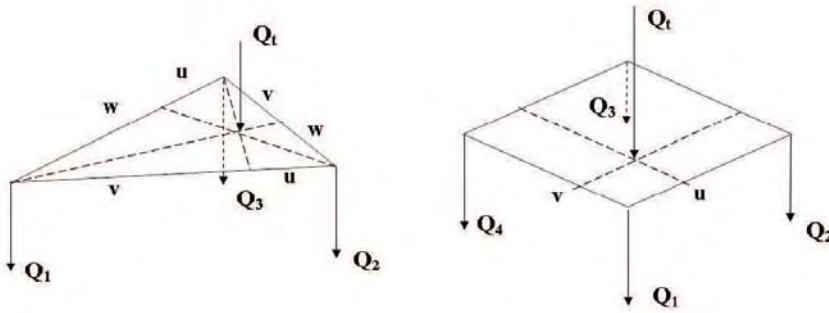


FIG. 3. Conservative interpolation. Data are interpolated from a single source point Q_t to the target points Q_i at the corners.

The first set is the EADS modules developed in frame of TAURUS project [28]. They are based on conservative solutions of finite elements, used to distribute the pressures from the CFD grid to the structural one (forces), and the displacements from the structural grid to the CFD grid.

The same goal could be obtained by the second set of modules employing the MpCCI [21] tools. MpCCI-based interpolation was successfully tested in Poznan University of Technology in frame of the TAURUS project [28].

The third set of modules is the in-house developed [29]. In the tools used by authors, bucket search algorithm has been used.

The comparison of all three sets of interpolating modules show no significant differences in performance and accuracy. They all allow interpolation between non-matching grids. EADS and in-house modules performed better in the cases, when only torsion box of the wing was modelled on the structural side. For further examples shown the EADS modules were used.

4.5. The description of the algorithm

In what follows, the simulation algorithm for static FSI calculations is presented (Fig. 4). The static computations are performed to specify initial conditions for a dynamic FSI analysis.

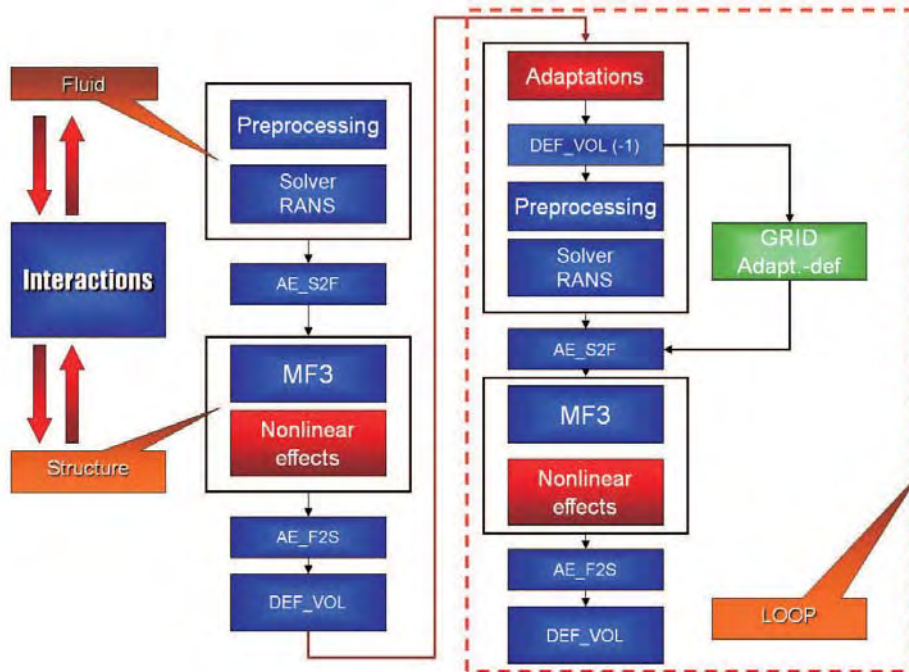


FIG. 4. The static FSI analysis, left – the starting point for adaptation a CFD grid.

In aeroelastic computations the structural model is subjected to the forces determined on the basis of pressure distribution computed with the CFD code. The analysis starts from CFD computation. The process consists of three stages. The first stage is about generating the consistent CFD grid (Fig. 5) and checking it for negative volumes and other grid pathologies. Then the grid is partitioned.

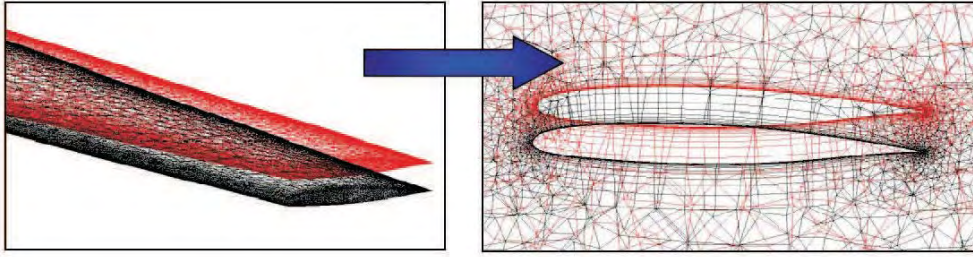


FIG. 5. An example of the CFD grid being deformed on the basis of the structural grid's displacement.

The division is dependent on the number of used processors, and in turn this number is dependent on the size of the task and the amount of time for the MPI packet to pass on messages.

The next stage constitutes a significant part of the flow analysis. The boundary conditions having been specified and the environment having been prepared, computations are performed. After the flow analysis, parameters for information exchange are specified (units, the coupling surface, object files).

Then the CFD data, in the form of the pressure distribution on the coupling surfaces, are translated into forces and interpolated from the CFD grid to the structural grid. The exchange occurs through the coupling surface, specified on the basis of the structural model and flow model.

The next step consists of structural calculations by means of structural code. Depending on settings, it is possible to perform a traditional linear analysis or to take into account the constitutive and geometrical nonlinearities. When the structural calculations have been completed, the information in the form of displacements of given nodes of the structural model is passed on to the deformation module. On the basis of the structure's displacement, the CFD grid is modified (Fig. 5), thus creating a new grid for the next step in the calculations. The process of deformation being realized is based on the spring analogy.

The designed tool also enables to perform dynamic analyses, what is necessary in analysing dynamic response of the aircraft depending on types of the input functions. In the case of dynamic simulations, the algorithm has been extended with an additional iterative loop (Fig. 6).

In this case, after introducing the initial condition (the input function), the dynamic response of the system to the initial perturbation in a given period of time is investigated. Dynamic aeroelastics also takes into account the acceleration of the structural grid (the grid's dynamics) and its impact on the flow. Information on the dynamics of the grid is obtained on the basis of cur-

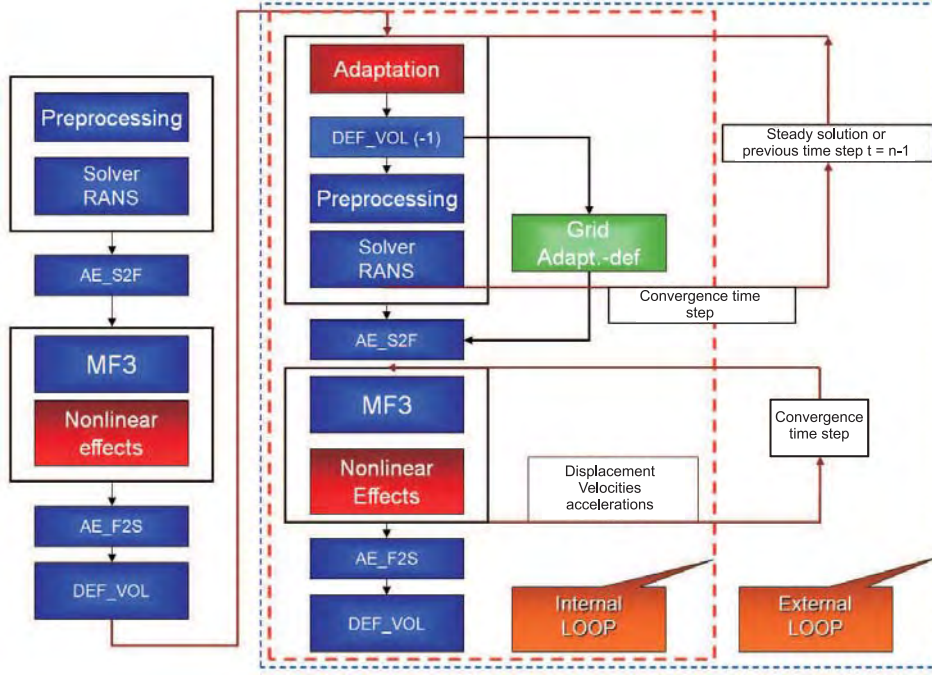


FIG. 6. The algorithm of dynamic FSI analysis.

rent displacements of the grid, in reference to the one obtained in the previous time step, as well as on basis of the previous flow solution. Typical time coupling procedures used for aeroelastic simulations are described in [30, 31]. Here the partitioned time stepping is used. The time coupling is solved explicitly as boundary conditions imposed by one system onto the other. To prevent numerical instability the time step is decreased and subiterations are performed. By subiterating the fully coupled solution is obtained. The size of time step for all the modules used is managed by CFD solver TAU-code, interfaced for this kind of aeroelastic computations in TAURUS project [28]. The description of similar management of aeroelastic time coupling can be found in [32].

5. A numerical simulation of the fluid-structure interaction for the chosen cases

5.1. A numerical simulation of the flow around NACA 0012 airfoil

The studies on flutter have proved that in models with linear characteristics, an infinite rise in amplitude can occur and the construction is destroyed in a short period of time. However, in systems in which non-linear springs have

been used in the suppression system after the critical speed has been reached, the amplitude of oscillation is set.

Simulation of aeroelasticity of non-linear structure is impossible with most of the standard aeroelastic codes destined for linear models. To simulate the experiment for the system having two degrees of freedom with non-linear restoring force, it was necessary to adapt the structural code and to rebuild the algorithm of fluid and structure interaction with each other.

A structural model has been created for the examined profile (Fig. 7) and a CFD grid has been generated (Fig. 8).

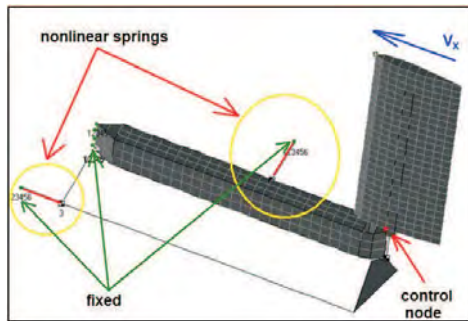


FIG. 7. The structural model of the NACA 0012 profile with non-linear springs used. The model complies with the experiment of IoA [33].

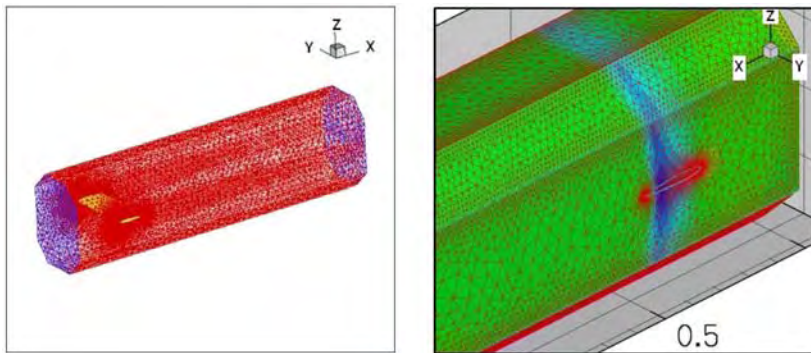


FIG. 8. A CFD grid for the NACA 0012 profile. Geometry of the domain reflects the experimental setting of the wind tunnel.

The CFD grid consisted of 1152587 tetrahedral elements and 197427 nodes. To achieve the most accurate results, comparable to the experiment, the accuracy of the structural model has been checked by comparing the eigenfrequencies assigned numerically with the ones determined experimentally.

Figure 9 shows the results of flow calculations for the dynamic FSI in the form of the velocity distribution towards the Y axis (inflow) for a linear case at the speed of $V_x = 28.2$ [m/s].

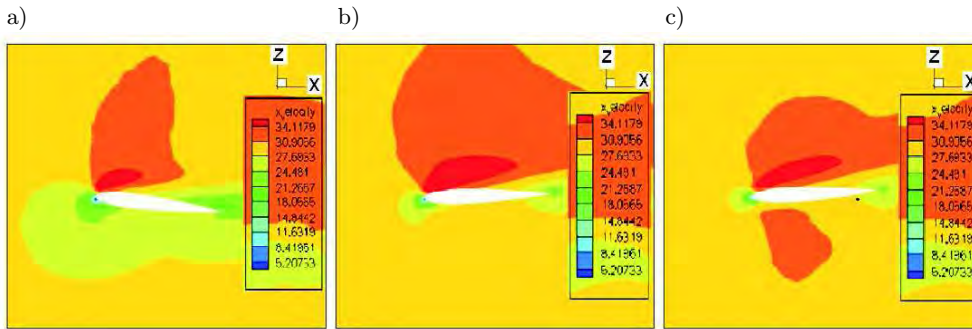


FIG. 9. The velocity distribution $V_x = 28.2$ [m/s] for: a) 1 time step; b) 10 time steps; c) 20 time steps.

A linear approach

Calculations have been made for the same configuration as in the case of the experimental studies. In the first stage of simulation, standard linear elements have been used. As a result, displacement and the angle of rotation in the function of time for specified boundary conditions have been obtained. Below one

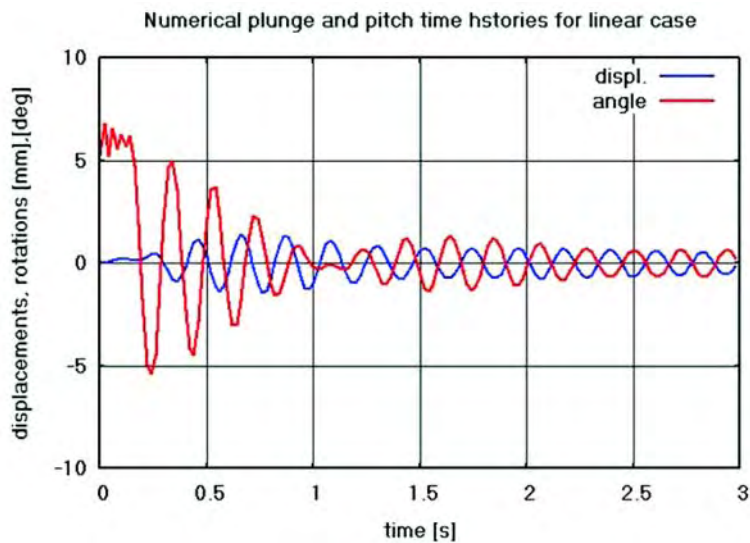


FIG. 10. Displacement and the angle of rotation (the control node) in the function of time for a linear case at the inflow speed of $V_x = 23$ [m/s].

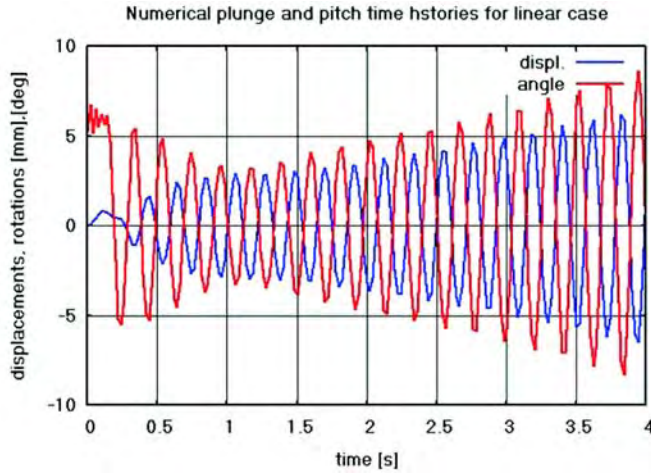


FIG. 11. Displacement and the angle of rotation (the control node) of the profile in a function of time – flutter’s critical speed – $V_F = 25$ [m/s].

can see sequences of displacement and the angle of rotation (the control node) as a function of time, obtained as a result of calculations by means of using linear elements (Figs. 10, 11).

Figure 10 shows the sequence of displacement and the angle of rotation of the control node in the function of time for an approximate inflow speed of 23 [m/s]. For the range of speed at which the flutter has occurred in experimental studies, the oscillations are decaying.

After increasing the speed to 25 [m/s] (Fig. 11), one can observe that the amplitude of the profile’s oscillation is growing rapidly in time. The critical flutter speed has been reached at 25 [m/s] for the numerical model, which agrees with the results of the experimental studies.

A non-linear approach

In the second stage of simulation, standard linear elements have been replaced with non-linear elements to simulate non-linear restoring force. As in the case of the previous simulation, MF3 code has been used to carry out a structural analysis, introducing procedures taking into account non-linearity.

Figure 12 shows the sequence of displacement and the control node rotation angle in the function of time for the inflow speed of 30 [m/s].

As one can see, considering the speed, the amplitude grew rapidly in the linear approach, what has been suppressed in the non-linear approach.

After increasing the speed to 33 [m/s] one could observe (Fig. 13) the profile’s oscillations with a similar amplitude as in the linear case.

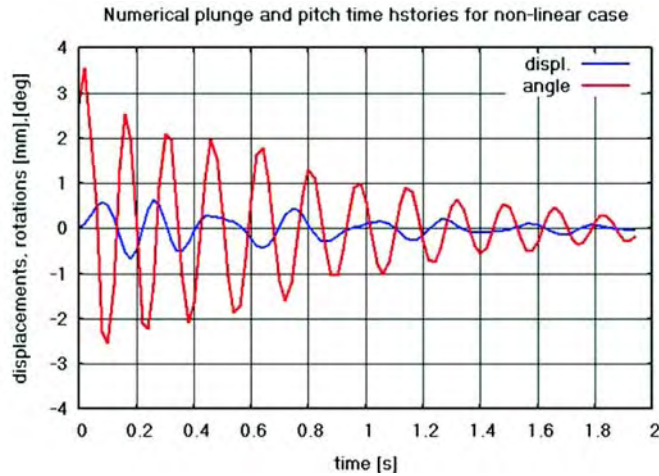


FIG. 12. Displacement and the profile's rotation angle (the control node) in a function of time for a non-linear case at the inflow speed of $V_x = 30$ [m/s].

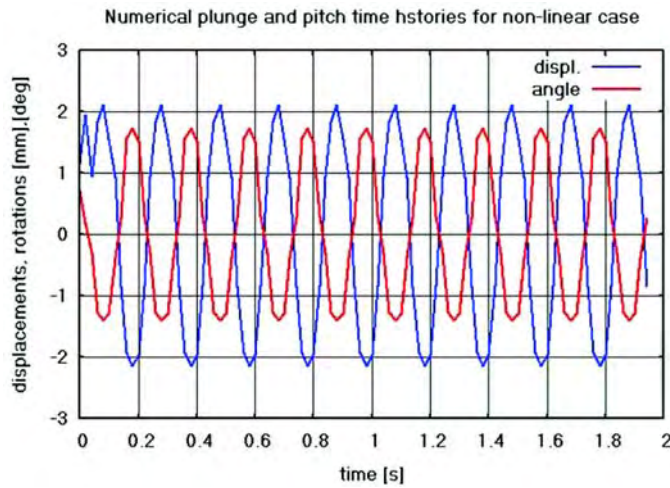


FIG. 13. Displacement and the profile's rotation angle (the control node) in a function of time for a non-linear case, at the inflow speed of $V_x = 33$ [m/s].

5.2. Summary

The results of numerical simulations compare fairly well with the experimental findings. The obtained results confirm the influence of structural non-linearity on the character of the fluid-structure system oscillations. There exists no complete theory accurately explaining the mechanism responsible for this process. It is particularly true for a coupled fluid-structure systems having very large number of degrees of freedom as the one used in the present paper. The more

detailed analysis is possible for a simplified dynamical system reduced to only few degrees of freedom, e.g. for the system two degrees of freedom with non-linear restoring force analyzed above. The methods of solution depend on the character and strength of non-linearity. The Harmonic Balance or High-Order Harmonic Balance [34] methods are often used for the analysis.

The Centre Manifold and Normal Form [35, 36] constitute the non-linear oscillator for the analyzed system. The form obtained with the Krylov–Bogoliubov ansatz and the use of cylindrical coordinates and normal forms [35] for the amplitude A and the phase ϕ are given by

$$(5.1) \quad \partial_t \mathbf{A} = \sigma_1 A + \beta A^3, \quad \partial_t \phi = \omega_1 + \gamma A^2,$$

with the growth rate σ_1 and the frequency ω_1 of the most unstable linear stability eigenmode, the Landau constant β , and the nonlinearity parameter γ .

The stability investigation of Eq. (5.1) determines the fix point – subcritical or supercritical Hopf bifurcation, related to flutter velocity. The character of bifurcation is related to the spring characteristics. The limit cycle of the dynamical system (Eq. (5.1)) is LCO in case of aeroelastic model. It is interesting to notice that the circular cylinder wake model in [37] deals with the same non-linear oscillator solution. The methodology used also by authors in flow modeling, like ROM analysis with POD of the snapshots, Galerkin Projection and dynamical system analysis, is often used to treat the high-dimensional aeroelasticity problems [38, 39]. As the ROM approach is aligned with the activity of the authors, formulation of low-dimensional model and identification of aeroelastic dynamical system is a target of further investigation.

5.3. A numerical simulation for given material models exemplified by the flexible delta profile

To carry out an analysis of the FSI for geometrical non-linearity and some non-linear material models (Mooney–Rivlin and Neo–Hookean [40]), a flexible delta wing [5] has been used (Figs. 14, 15), which has been subjected to deformation in a linear case, and using non-linear material properties in a non-linear case.

The structural model has been created in CAD system (Fig. 14). It is consisting of 3543 shell elements having the following properties:

- thickness: $T = 10$ [mm],
- Young’s module $E = 6.9e + 05$ [Pa],
- Poisson’s ratio $\nu = 0.3$,
- density: $\rho = 2700$ [kg/m³].

Boundary conditions have been specified in the form of restraint in line with the experimental data [6]. The next step in preparing the FSI calculations was to

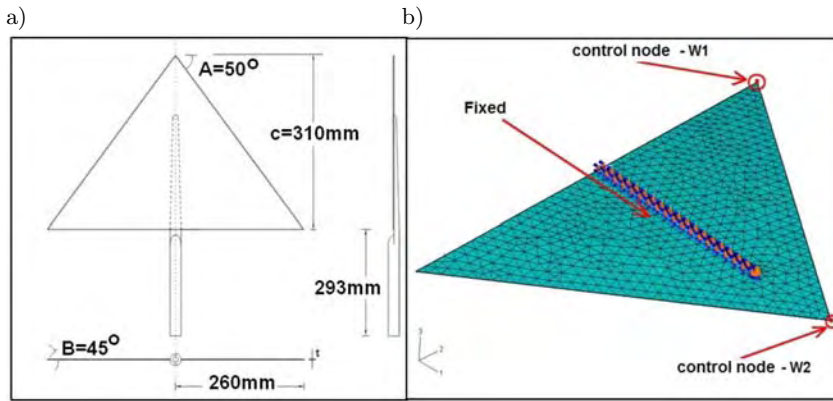


FIG. 14. A flexible delta wing: a) geometry [5], b) a structural grid with applied boundary conditions.

generate a three-dimensional CFD grid for the URANS analysis (Fig. 15). The grid consists of 3050400 tetrahedral elements, 45045 prismatic elements and 152 regular tetrahedron-like elements.

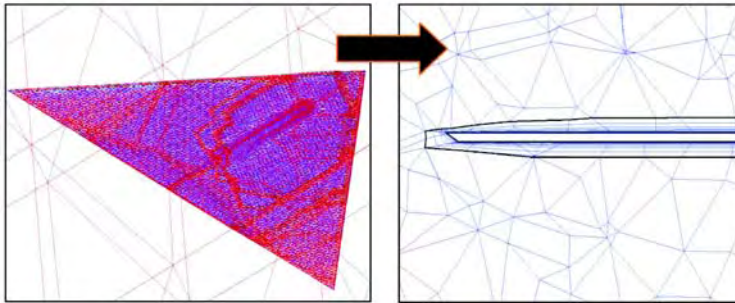


FIG. 15. A flexible delta wing – a CFD grid for the URANS analysis.

The grid generated in that way has been tested to check grid connectivity and the quality of particular elements.

An analysis of the FSI has been performed for the following boundary conditions, parameters and turbulence model:

- inflow speed $V_x = 5, 10, 15, 20$ [m/s],
- atmospheric pressure $P = 0.1$ [MPa],
- Reynolds number $Re = 620\,000$,
- angle of attack $\alpha = 100$,
- time step $t = 0.01$ [s],
- turbulence model: LEA $k - \omega$.

5.3.1. A flexible delta wing with the linear approach. In the first stage of the numerical simulation, linear material has been used for the flexible delta wing in line with the assumptions specified above. In Fig. 16 one can see the results of the calculations of displacement for the control nodes W1 and W2 of the structural model in the function of time for the inflow speed of 20 [m/s], at which a rapid increase in amplitude of displacement has been observed in the function of time in the linear case. The results for the remaining speeds can be found in [20]. As a result of the calculations made for the first inflow speed $V_x = 5$ [m/s] [20], the amplitude of the examined profile's displacements specified in the W1 and W2 control nodes has risen slightly. Calculations have been repeated to verify the results obtained for this and other cases.

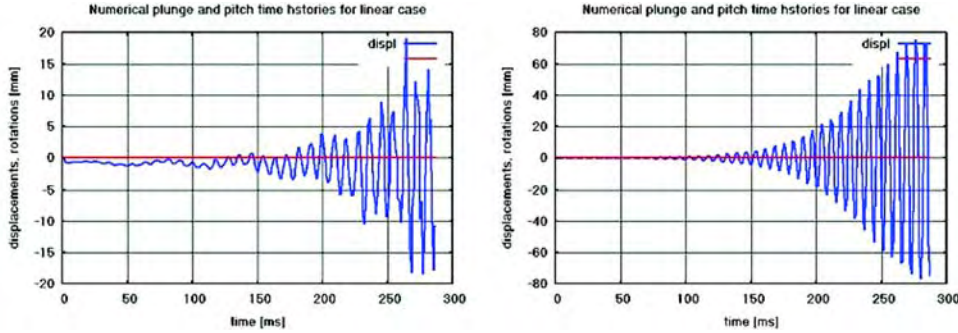


FIG. 16. Displacements of control nodes in function of time, in the linear case at the inflow speed of $V_F = 20$ [m/s]: a) W1 node, b) W2 node.

As the inflow speed is increased to 20 [m/s] the amplitude of displacement (Fig. 16) shows that the critical speed of the flutter has been obtained. Oscillations grew rapidly in line with the value at which a real model would be deformed or even destroyed in the final stage.

5.3.2. A flexible delta wing with the Mooney–Rivlin non-linear model. The next stage of the numerical simulation, consisted in using the Mooney–Rivlin non-linear material model for a flexible data wing. In order to be able to compare linear and non-linear models, initial parameters have been specified as in the case of linear material.

- thickness: $T = 10$ [mm],
- constants: $C_{10}, C_{01} = 6.9e + E05$ [Pa],
- density: $\rho = 2700$ [kg/m³].

Simulations for specific inflow speeds: 5, 10, 15, 20 [m/s] have been made in an analogous way. Below one can find the results for the W1 and W2 nodes displacement calculations for the structural model (Fig. 17) in the function of time, with the inflow speed of 20 [m/s].

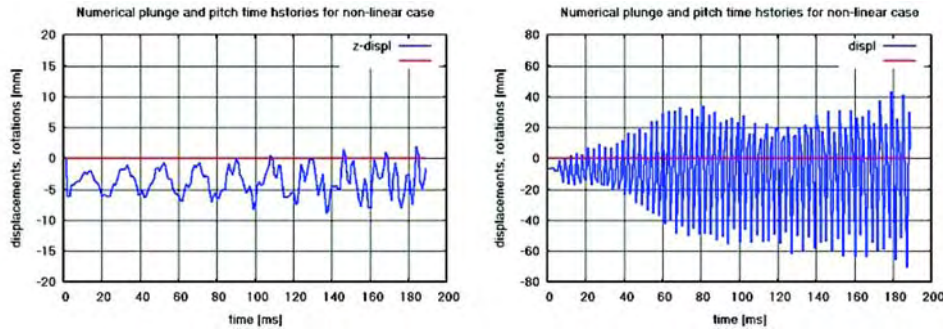


FIG. 17. Displacements of the control nodes in the function of time in the non-linear case of Mooney–Rivlin material model at the inflow speed of $V_x = 20$ [m/s]: a) W1 node, b) W2 node.

For linear case at the speed of 20 [m/s] (Fig. 17), exponential rise in the amplitude indicating flutter is observed. For the same conditions the nonlinear model exhibits LCO with saturation of the oscillation amplitude.

5.3.3. A flexible delta wing with the Neo–Hookean non-linear model. The last stage of the numerical simulation was to use the Neo–Hookean material model for a flexible delta wing. The model is employed with loads smaller than in the case of the Mooney–Rivlin material model. In this case the initial parameters were the same as for linear materials:

- thickness: $T = 10$ [mm],
- constant: $C_{10} = 6.9e + E05$ [Pa],
- density: $\rho = 2700$ [kg/m³].

As in the linear case, the inflow speeds of 5, 10, 15, 20 [m/s] were set in the Mooney–Rivlin non-linear model.

As it can be seen from the results depicted in Fig. 18, for the inflow velocity 20 [m/s] the amplitude of the oscillation saturates at the value larger than

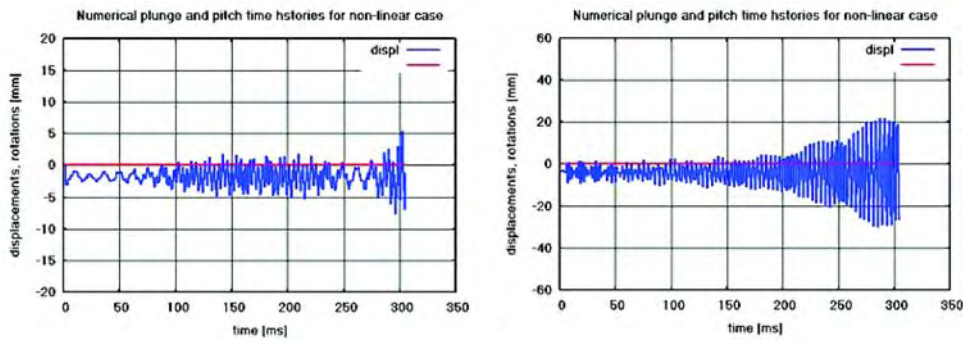


FIG. 18. The control nodes displacements in the function of time for the Neo–Hookean non-linear material model at the inflow speed of $V = 20$ [m/s]: a) W1 node, b) W2 node.

in the previous, Mooney–Rivlin case. However, also in this case the LCO is present.

5.3.4. Summary. The simulation shown above for the system having only 2 degrees of freedom and the experiments [33] for the NACA 0012 profile show that the nonlinearity changes considerably the FSI nature. The same conclusion can be drawn for non-linear material models (Mooney–Rivlin’s and Neo–Hookean) with continuous structural models. The developed tool enable analyses for hybrid structural models consisting of both linear and non-linear materials. The nonlinear FSI computation shown here are targeting practical problems encountered in aviation industry. To demonstrate the applicability of the system for industrial applications, the real-life configuration has to be considered. For this purpose the full configuration of I23 plane (Fig. 19) has been chosen.

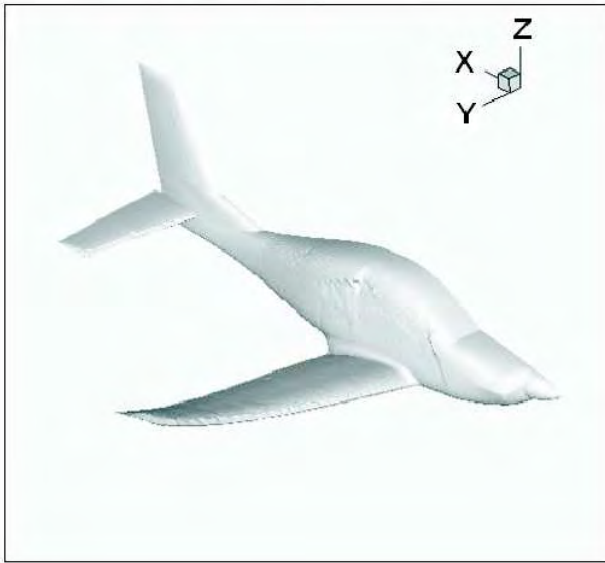


FIG. 19. The I23 model.

5.4. A simulation of the FSI exemplified by the I23 plane

The structural model has been obtained in cooperation (in frame of TAURUS project and later) with the Institute of Aviation in Warsaw (Fig. 20, left). The model consists of beam and mass elements.

The boundary conditions have been specified in line with the data from the Institute of Aviation. To perform the computations, the three-dimensional non-structural CFD grid has been generated (Fig. 20, right). The grid consists of about 15 millions of tetrahedral elements.

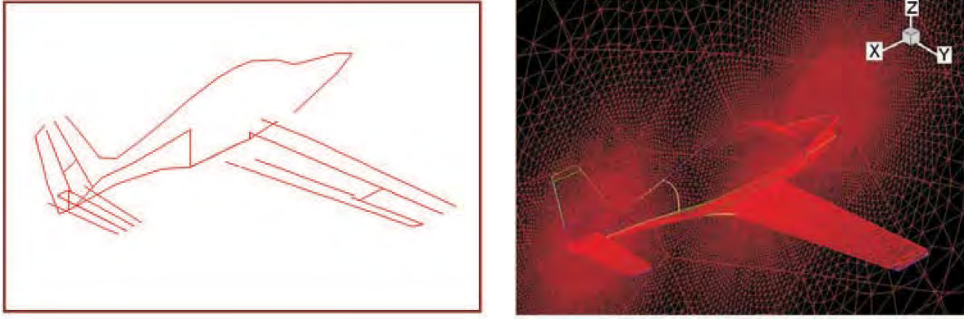


FIG. 20. A discrete model of the I23 plane for structural and flow analyses.

The grid generated in this way has been subjected to quality tests. The FSI has been carried out for the following boundary conditions and parameters:

- Mach number $Ma = 0.3$,
- atmospheric pressure $P = 0.1$ [MPa],
- Reynolds number $Re = 2 \cdot 10^6$,
- angle of attack $\alpha = 0.026$,
- time step $t = 0.01$ [s],
- singular input function: $F_z = 2000$ [N] in time $t = 0.01$ [s].

The FSI analyses of the I23 has been carried out for both, static and dynamic conditions. The result of the static FSI analysis was input into the dynamic one. The perturbation is introduced as the impulse force on the wing tip. The results of the analysis are shown in the following figures.

Figure 21 shows the displacement of the CFD grid for the I23 plane in consecutive stages of the analysis.

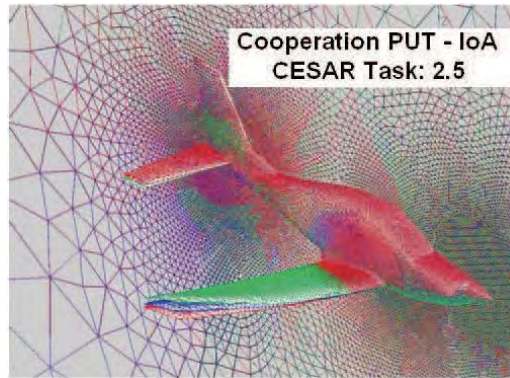


FIG. 21. An example of the CFD grid deformation on the basis of the structural grid.

The above-discussed system predicts correctly FSI phenomena, e.g. the flutter, which are particularly important during designing and certifying planes. Figure 21 shows static FSI plane deformation.

In Fig. 22 the sequence of plane deformations for subsequent time steps is depicted. In the figure, the flutter originating on the plane wing can be clearly seen.

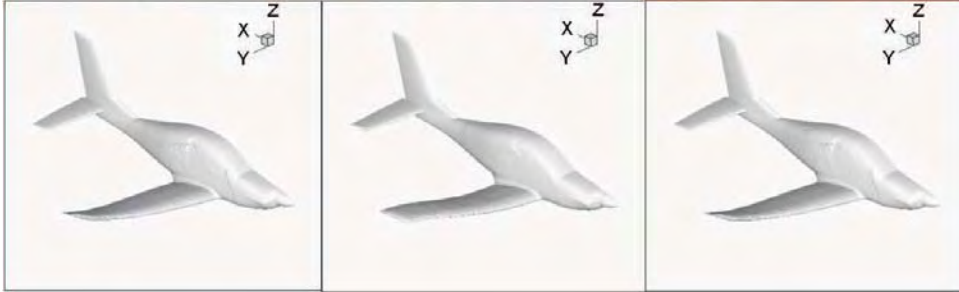


FIG. 22. The I32 plane wing deformation for a aerodynamic analysis of the flutter.

As a result of the calculations being made for the inflow speed $Ma = 0.3$, the displacement amplitude (Fig. 23) shows that the critical speed of the flutter has been reached. Oscillations grew rapidly, a real model would be deformed permanently or even destroyed.

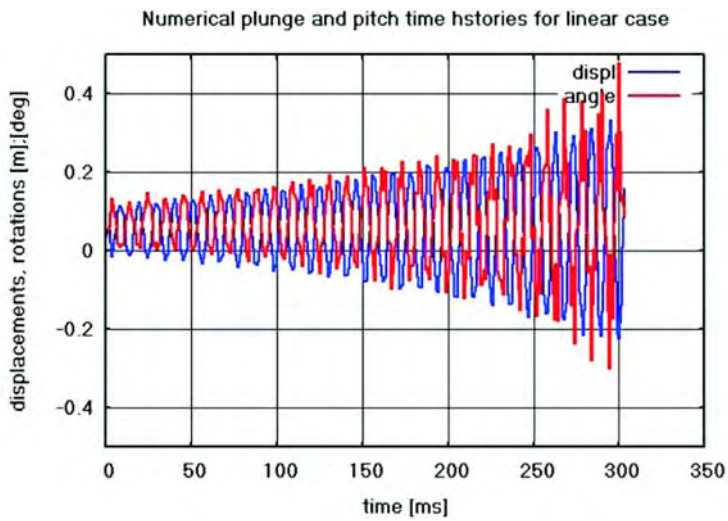


FIG. 23. Displacement of the control point lying at the tip of the I23 plane wing in function of time, with the flutter occurring.

6. Conclusions

The system for large-scale aeroelastic simulation with material nonlinearity has been developed. The test computations, performed for simple 2 degrees of freedom, plunging and pitching NACA0012 airfoil with non-linear restoring force, compare fairly well with the experiment. The results of the computational analysis prove that using non-linear material models (Mooney–Rivlin’s and Neo–Hookean) in a structural model, changes considerably the nature of phenomena found during the flow around of an examined profile. In the case of both the Mooney–Rivlin and Neo–Hookean non-linear material models, the LCO has been obtained. The flutter has occurred in the linear case. Results were obtained also for large deflection of the structure. This confirms that the system can handle not only material but also geometrical nonlinearity. Finally, the computations of the full-configuration aircraft have been performed. Large-scale, non-linear, industry-oriented aeroelastic computations are feasible with the presented system. The I23 plane’s analysis shows that the presented here numerical tool can be used in design process in the aviation industry as well as in examining dangerous phenomena, such as the flutter limit-cycle oscillation (LCO). Introducing the non-linear damping matrix to the system will be a natural direction of development. It will enable extending the scope of practical usefulness in modeling of active control over aeroelastic phenomena.

Acknowledgments

The authors would like to acknowledge Norbert Kroll and Deutsches Zentrum für Luft- und Raumfahrt (DLR) for providing us updated version of the TAU-code, Luciano Fornasier (EADS) for help in improvement of the code, Institute of Aviation Warsaw team for professional assistance and test case data (Wojciech Potkanski, Antoni Niepokulczycki, Daniel Szelag, Zbigniew Lorenc), Frank Thiele and Bernd R. Noack (TU-Berlin) for stimulating discussions.

References

1. P. POSADZY, M. MORZYŃSKI, Deliverable D5.2-24 – Final report on functionality of the implemented generic CSM code (Milestone M8), Technical report, Poznan University of Technology, 2004.
2. R. KAMAKOTI, *Computational Aeroelasticity Using a Pressure-Based Solver*, PhD thesis, University of Florida, 2004.
3. R.L. BISPLINGOFF, H. ASHLEY, R.L. HALFMAN, *Aeroelasticity*, Addison Wesley, Reading, MA, 1955.

4. S.N. ATLURI, S. SHEN, *The meshless local Petrov-Galerkin (MLPG) method: a simple and less-costly alternative to the finite element and boundary element method*, CMES: Computer Modeling in Engineering and Sciences, **3**, 1, 11–52, 2002.
5. G.P. GURUSWAMY, C. BYUN, *Fluid-structure interactions using Navier-Stokes flow equations coupled with shell finite element structures*, [in:] 24th Fluid Dynamics Conference, Orlando, FL, July 1993, AIAA-93-3087.
6. R. ROSZAK, *Fluid-structure interaction for nonlinear property of structural models*, PhD thesis, Poznan University of Technology, 2006.
7. S. PIPERNO, C. FARHAT, B. LARROUTUROU, *Partitioned procedures for the transient solution of coupled aeroelastic problems Part I: Model problem, theory and two-dimensional application*, Computer Methods in Applied Mechanics and Engineering, **124**, 1–2, 79–112, 1995.
8. C. FARHAT, M. LESOINNE, N. MAMAN, *Mixed Explicit/Implicit Time Integration of Coupled Aeroelastic Problems: Three-field Formulation, Geometric Conservation and Distributed Solution*, International Journal for Numerical Methods in Fluids, **21**, 807–836, 1995.
9. S. PIPERNO, *Explicit/implicit fluid/structure staggered procedures with a structural prediction and fluid subcycling for 2D inviscid aeroelastic simulations*, International Journal for Numerical Methods in Fluids, **25**, 1207–1226, 1997.
10. D. SCHWAMBORN, T. GERHOLD, R. HEINRICH, *The DLR TAU-Code: Recent Applications in Research and Industry*, [in:] Proceedings of ECCOMAS CFD, 2006.
11. C. FARHAT, C. DEGAND, B. KOOBUS, M. LESOINNE, *Torsional springs for two-dimensional dynamic unstructured fluid mesh*, Comput. Methods Appl. Mech. Engg., **163**, 231–245, 1998.
12. C. DEGAND, C. FARHAT, *A three-dimensional torsional spring analogy method for unstructured dynamic meshes*, Comput. Struct., **80**, 305, 2002.
13. F.J. BLOOM, *Consideration on the spring analogy*, Int. J. Numer. Methods Fluids, **32**, 647–668, 2000.
14. D. ZENG, C.R. ETHIER, *A semi-torsional analogy model for updating unstructured meshes in 3D moving Domains*, Finite Elem. Anal. Des., **41**, 1118–1139, 2005.
15. G.A. MARKOU, Z.S. MOUROUTIS, D.C. CHARMPIS, M. PAPADRAKAKIS, *The ortho-semi-torsional (OST) spring analogy method for 3D mesh moving boundary problems*, Comput. Methods Appl. Mech. Engg., **196**, 747–765, 2007.
16. C.L. BOTTASANO, D. DETOMI, R. SERRA, *The ball-vertex method: a new simple analogy method for unstructured dynamic meshes*, Comput. Methods Appl. Mech. Engg., **194**, 4244–4264, 2005.
17. M. MORZYŃSKI, *Numerical solution of Navier-Stokes equations by the finite element method*, [in:] Proceedings of SYMKOM 87, Compressor and Turbine Stage Flow Path – Theory and Experiment, 119–128, 1987.
18. K. APPA, *Finite-surface spline*, Journal of Aircraft, **26**, 495–496, 1989.
19. R.L. HARDER, R.N. DESMARIS, *Interpolation using surface splines*, Journal of Aircraft, **9**, 2, 189–191, 1972.

20. C. FARHAT, M. LESOINNE, *Two efficient staggered algorithms for the serial and parallel solution of three-dimensional nonlinear transient aeroelastic problems*, Comput. Methods Appl. Mech. Engrg., **182**, 499–515, 2000.
21. MpCCI 2.0 User Guide, Technical report.
22. N. MAMAN, C. FARHAT, *Matching fluid and structure meshes for aeroelastic computations*, Computers and Structures, **54**, 4, 779–785, 1995.
23. D. KNUTH, *Sorting and Searching. The Art of Computer Programming, Vol. 3*, Addison-Wesley, Massachusetts 1973.
24. R. LÖHNER, *Some useful data structures for the generation of unstructured grids*, Applied Numerical. Math, **4**, 123–135, 1988.
25. D.J. BENSON, J.O. HALLQUIST, *A Single surface contact algorithm for the post-buckling analysis of shell structures*, Comput. Methods Appl. Mech. Engrg., **78**, 141–163, 1990.
26. Y. KUO, S.-Y. HWANG, H. HU, *A data structure for fast region searches*, IEEE Design and Test of Computers, **6**, 5, 20–28, 1989.
27. T. ASANO, M. EDAHIRO, H. IMAI, M. IRI, K. MUROTA, *Practical use of bucketing techniques in computational geometry*, 1985, 153–195, [in:] G.T. TOUSSAINT [Ed.], Computational Geometry, Vol. 2: Machine Intelligence and Pattern Recognition, North-Holland, Amsterdam.
28. Technology development for aeroelastic simulations on unstructured grids, Fifth E.U. Framework Programme, G4RD-CT-2001-00403, <http://cordis.europa.eu>.
29. P. POSADZY, *The modelling and analysis of aeroelasticity phenomena in practical flow applications* [in Polish], PhD thesis, Poznan University of Technology, 2007.
30. S. PIPERNO, C. FARHAT, *Partitioned procedures for the transient solution of coupled aeroelastic problems – Part II: energy transfer analysis and three-dimensional applications*, Computer Methods in Applied Mechanics and Engineering, **190**, 24–25, 3147–3170, 2001.
31. C. FARHAT, M. LESOINNE, P. STERN, S. LANTÉRI, *High performance solution of three-dimensional nonlinear aeroelastic problems via parallel partitioned algorithms: methodology and preliminary results*, Advances in Engineering Software, **28**, 1, 43–61, 1997.
32. L. FORNASIER, H. RIEGER, U. TREMEL, E. VAN DER WEIDE, *Time-Dependent Aeroelastic Simulation of Rapid Manoeuvring Aircraft*, AIAA Paper, **949**, 2002.
33. D. SZELAG, Z. LORENC, L. FORNASIER, P. POSADZY, *A digitally controlled suspension system for the real time generation of the structural nonlinearities in the flutter wind tunnel validation testing*, [in:] Proceedings of the International Forum on Aeroelasticity and Structural Dynamics, Munich, Germany 2004.
34. L. LIU, E.H. DOWELL, J.P. THOMAS, *A high dimensional harmonic balance approach for an aeroelastic airfoil with cubic restoring forces*, Journal of Fluids and Structures, **23**, 3, 351–363, 2007.
35. B.D. COLLIER, P.A. CHAMARA, *Structural non-linearities and the nature of the classic flutter instability*, Journal of Sound and Vibration, **277**, 4–5, 711–739, 2004.
36. Y. CHEN, J. LIU, *Supercritical as well as subcritical Hopf bifurcation in nonlinear flutter systems*, Applied Mathematics and Mechanics, **29**, 2, 199–206, 2008.

37. B.R. NOACK, K. AFANASIEV, M. MORZYŃSKI, G. TADMOR, F. THIELE, *A hierarchy of low-dimensional models for the transient and post-transient cylinder wake*, J. Fluid Mech., **497**, 335–363, 2003.
38. S. MUNTEANU, J. RAJADAS, C. NAM, A. CHATTOPADHYAY, *Reduced-order-model approach for aeroelastic analysis involving aerodynamic and structural nonlinearities*, AIAA Journal, **43**, 3, 560–571, 2005.
39. T. KIM, H. HONG, K.G. BHATIA, G. SENGUPTA, *Aeroelastic Model Reduction for Affordable Computational Fluid Dynamics-Based Flutter Analysis*, AIAA Journal, **43**, 12, 2487, 2005.
40. P. BJORNSSON, H. DANIELSSON, *Strength and Creep Analysis of Glued Rubber Foil Timber Joints*, Master's thesis, Lund University, Sweden 2005.

Received June 6, 2008; revised version January 27, 2009.
